

A New Machine Learning Approach Based on Range Corrected Deep Potential Model for Efficient Vibrational Frequency Computation

Jitai Yang, Yang Cong, and Hui Li*

Institute of Theoretical Chemistry, College of Chemistry, Jilin University, 2519 Jiefang Road, Changchun 130023, P.R.China

E-mail: Prof_huili@jlu.edu.cn

Abstract

Vibrational spectrum simulation, as an ensemble average result, can be very time consuming when using high accuracy methods. Here, we introduce a new machine learning approach based on the range corrected deep potential (DPRc) model to improve computing efficiency. The approach was applied to computing C=O stretching vibrational frequency shifts of formic acid-water solution. DPRc is adapted for frequency shift calculation. The system was divided into “probe region” and “solvent region” by atom. Three kinds of “probe region” were tested: single atom with atomic contribution correction, a single atom, and a single molecule. All data sets were prepared using by Quantum Vibration Perturbation (QVP) approach. The deep potential (DP) model was also adapted for frequency shift calculation for comparison, and different interaction cut-off radii were tested. The single molecule “probe region” results show the best accuracy, running roughly ten times faster than regular DP, while reducing the training time by a factor of about four, making it fully applicable in practice. The results show

that dropping information of interaction distances between solvent atoms can significantly increase computing and training efficiency while ensuring little loss of accuracy. The protocol is practical, easy to apply, and extendable to calculating other physical quantities.

1 Introduction

Vibrational spectroscopy is a powerful experimental detection technique used in various systems, including molecular clusters, solids, solutions, proteins, and surface systems.¹⁻⁷ With the help of theoretical simulations, experimental spectra can be interpreted and gain additional insights such as dynamic spectral diffusion, vibrational quantum effects, and the complexity of the environment at the atomic level. Ensemble average must be performed if explicitly considering the dynamic and complex chemical environment around the chromophore. The average can be either based on a single chromophore or from a group consisting of all molecules. Because there are fewer atoms when starting with a single chromophore molecule, higher precision and more rigorous treatment can be utilized, and then undertake more analysis from a molecular view, such as solvatochromism and combining hydrogen bond analysis. However, introducing high precision or rigorous methods limits computing efficiency, and approximations must be reintroduced.⁸⁻¹³

The Quantum Vibration Perturbation (QVP) approach is accurate and can handle the molecular quantum vibrational effect in complex systems.¹⁴⁻¹⁸ Using contracted and localized basis from potential optimized discrete variable representation (PODVR),¹⁹ the QVP approach is affordable in picosecond time scale or calculating tens of thousands of frequencies but still challenging in nanosecond time scale. Multi-dimension vibrational modes coupling problem also poses rigorous efficiency requirements.

In particular, due to the development of the versatility of machine learning in recent years, machine learning methods can also be introduced to solve the efficiency problem in computational chemistry. Many models have been created for potential calculation and take

functions of atom coordinates as their inputs. Naturally, these methods can be expanded to compute other physical quantities. In this work, we are interested in vibrational frequencies and there have been many related studies.²⁰⁻²⁵ Using artificial neural networks (ANN) with atom-centered symmetry functions (ACSFs), Kananenka et al. reduced their map method’s errors by more than 25 cm^{-1} . The final errors were still higher than that of later methods.²⁵ Kwac and Cho used feed-forward neural network (FFNN) and convolutional neural network (CNN) models on a relatively small dataset (4500 data points) to describe the frequency shifts of the amide I mode vibration of *N*-methylacetamide (NMA) in water, where CNN performs better than FFNN does, with the best result of 8.56 cm^{-1} . However, the training curve showed that CNN ran into overfitting problem quickly. The small data size possibly caused this. For FFNN models, the RMSE showed a steady and slow decline during training, and the result was good with 8.91 cm^{-1} .²⁰ Kwac et al. then applied FFNN to the OH stretch vibration of water with a same size dataset and obtained results with similar accuracy.²⁶ Ye et al. applied multi-layer perceptron (MLP) and Coulomb matrix (CM) to calculate neighboring couplings and frequencies of amide I in the protein system, achieved a high accuracy of less than several wavenumbers with harmonic approximation.²³

Considering individual chromophores in chemical surroundings, a natural idea is to focus on the effect of the surrounding environment on them, in which the interactions between the chromophore atoms and chromophore atoms with surrounding atoms are the most important, followed by the interaction between the environmental atoms. Additionally, for nonbonded interactions between neutral molecules, the effective distance is limited and is generally considered to be about 10 Å . Many works have tried to treat the interactions of different atoms separately, but their interaction cut-off radii are usually around 6 Å .^{20,23,25} This picture is very similar to the one encountered in the quantum mechanical/molecular mechanical (QM/MM) method,^{27,28} and the deep potential range-corrected (DPRc) method is a machine learning method developed for computing the QM/MM energy correction which able to treat the interactions separately. As far as we know, there has yet to be any work on spectrum

simulation utilizing the DPRc model.

In this work, we present a new machine learning approach based on DPRc to calculate the instantaneous vibrational frequency shifts of individual chromophores by structure. Different interaction divisions and interaction cut-off radii (6 Å and 10 Å) were tested. All data sets were prepared using by QVP approach. The deep potential (DP) model was also adapted for shift calculation for comparison.

2 Method

2.1 Quantum vibration perturbation (QVP)

The semi-classical equation is often used to compute the infrared (IR) spectral lineshape $I(\omega)$ ²⁹

$$I(\omega) \propto \Re \int_0^\infty dt e^{i\omega t} \left\langle \mathbf{m}(t) \mathbf{m}(0) e^{-i \int_0^t d\tau \left\{ \omega(\tau) - \frac{i}{2T_1(\tau)} \right\}} \right\rangle \quad (1)$$

where \mathbf{m} is vibrational transition dipole moment, T_1 is relaxation time of the vibration, and the large angular brackets denote an ensemble average, $\omega(t)$ is instantaneous time-dependent vibrational frequencies. Usually, T_1 value is from experiment, with Condon approximation, the magnitude of \mathbf{m} is fixed, and its orientation is taken as the vector of the vibrational mode. By molecular dynamic simulation, solvent dynamics is modeled classically. The time-dependent instantaneous frequency $\omega(t)$ of the probe molecule can be treated quantum mechanically.

At first, we build reference quantum vibrational states. The Cartesian coordinates of chromophore is expanded in terms of the normal mode vectors, $\boldsymbol{\xi}_i (i = 1, 2, \dots, N - 6)$, with respect to equilibrium geometry \mathbf{R}_e .

$$\mathbf{R}^{\text{ch}} = \mathbf{R}_e + \sum_i Q_i \boldsymbol{\xi}_i \quad (2)$$

where \mathbf{R}^{ch} is the Cartesian coordinates of a nonlinear chromophore and $Q_i (i = 1, 2, \dots, N - 6)$

are the $N - 6$ vibrational coordinates. We usually focus on a specific mode ξ_s , The potential energy as a function of the mode ξ_s is given by

$$\hat{V}_0 = V_0(Q_s) = E_{\text{BO}}(\mathbf{R}_e + Q_s \xi_s) \quad (3)$$

Q_s is the normal-mode coordinate and E_{BO} indicates the Born-Oppenheimer potential energy determined by an ab initio method. The one-dimension vibration Schrödinger equation is solved with DVR³⁰ and PODVR. Then an isolated chromophore is chosen as the reference states. Next, we embed the vibrational degrees of freedom into the sample frames of molecular dynamics (MD) trajectory, where the dynamic chemical environment is added. Then instantaneous vibrational frequencies are obtained by Rayleigh-Schrödinger Perturbation Theory (RSPT). The perturbation can be written as follows

$$\hat{V}' = V'(t; Q_s) = E_{\text{BO}}(\mathbf{R}(t; Q_s)) - E_{\text{BO}}(\mathbf{R}_e + Q_s \xi_s) \quad (4)$$

The corresponding transition frequency ω^1 between the first excited and ground states at first-order perturbation (QVP1) is given by

$$\begin{aligned} \omega^1(t) &= E_1^0 - E_0^0 + \langle \phi_1 | \hat{V}' | \phi_1 \rangle - \langle \phi_0 | \hat{V}' | \phi_0 \rangle \\ &= \Delta E^0 + \int dQ_s \Delta \rho_s(Q_s) V'(t; Q_s) \\ &= \Delta E^0 + \sum_{i=1}^{N^{\text{PO}}} dQ_{s,i} \Delta \rho_s(Q_{s,i}) V'(t; Q_{s,i}) \end{aligned} \quad (5)$$

$\Delta \rho_s$ is the density difference between the first excited and ground states. The integral is converted to summation in PODVR fashion. Finally, the lineshape can be calculated by the transition frequency $\omega^1(t)$, in other words, instantaneous time-dependent vibrational frequency shifts $\Delta \omega$ from ω of reference states. More details about QVP can be checked in our previous work.^{14,18}

2.2 Deep potential range correction (DPRc) for frequency shift computing

DPRc was originally designed to handle the energy calculations in QM/MM. Here, we restate the relevant theory in the frequency shift calculation task context. More details about DPRc for QM/MM can be found in the work of Zeng et al.³¹

In DP model, the final result is a sum of atomic contributions. Instead of energy, the physical quantity here is the vibrational frequency shift.

$$S = \sum_{i=1}^N S_i \quad (6)$$

$$S_i = \mathcal{N}(D(\tilde{\mathcal{R}})) \quad (7)$$

The atomic contribution S_i is a neural network consisting of hidden layers \mathcal{N} , the number and specific form of which are determined by the parameter settings in the input file. $D(\tilde{\mathcal{R}})$ is the input layer and the “descriptor” array which contains a local embedding network to reduce the dimensions in $\tilde{\mathcal{R}}$.³²

$\tilde{\mathcal{R}}$ is the “environment matrix”:

$$(\tilde{\mathcal{R}}_i)_{ja} = \begin{cases} s(R_{ij}), & \text{if } a = 1 \\ s(R_{ij})X_{ij}/R_{ij}, & \text{if } a = 2 \\ s(R_{ij})Y_{ij}/R_{ij}, & \text{if } a = 3 \\ s(R_{ij})Z_{ij}/R_{ij}, & \text{if } a = 4 \end{cases} \quad (8)$$

$s(R_{ij})$ is a switched reciprocal distance function that controls the range of the environment

to be described.

$$s(R_{ij}) = \begin{cases} \frac{1}{R_{ij}}, & \text{if } R_{ij} \leq R_{\text{on}} \\ \frac{1}{R_{ij}} \left\{ \left(\frac{R_{ij}-R_{\text{on}}}{R_{\text{off}}-R_{\text{on}}} \right)^3 \left(-6 \left(\frac{R_{ij}-R_{\text{on}}}{R_{\text{off}}-R_{\text{on}}} \right)^2 + 15 \frac{R_{ij}-R_{\text{on}}}{R_{\text{off}}-R_{\text{on}}} - 10 \right) + 1 \right\}, & \text{if } R_{\text{on}} < R_{ij} < R_{\text{off}} \\ 0, & \text{if } R_{ij} \geq R_{\text{off}} \end{cases} \quad (9)$$

If a neighboring atom is within a distance of R_{on} , the atom will have full weight. The weight smoothly changes between R_{on} and R_{off} .

In the initial design for QM/MM approach, the model is responsible for the correction of interactions between QM atoms with other QM atoms and with nearby MM atoms. Similarly, in the frequency shift calculations, we expect the model to focus on interactions between chromophore atoms with other chromophore atoms and with nearby solvent atoms. In order to meet the demand, we divide the system into "probe region" and "solvent region", and deal with the interactions base on different regions in the switching function:

$$s_{ij}(R_{ij}) = \begin{cases} 0, & \text{if } ij \in \text{Solvent} \\ \frac{1}{R_{ij}}, & \text{if } ij \in \text{Probe} \\ \text{if } i \in \text{Probe} \wedge j \in \text{Solvent} \text{ or } i \in \text{Solvent} \wedge j \in \text{Probe} : \\ \frac{1}{R_{ij}}, & \text{if } R_{ij} \leq R_{\text{on}} \\ \frac{1}{R_{ij}} \left\{ \left(\frac{R_{ij}-R_{\text{on}}}{R_{\text{off}}-R_{\text{on}}} \right)^3 \left(-6 \left(\frac{R_{ij}-R_{\text{on}}}{R_{\text{off}}-R_{\text{on}}} \right)^2 + 15 \frac{R_{ij}-R_{\text{on}}}{R_{\text{off}}-R_{\text{on}}} - 10 \right) + 1 \right\}, & \text{if } R_{\text{on}} < R_{ij} < R_{\text{off}} \\ 0, & \text{if } R_{ij} \geq R_{\text{off}} \end{cases} \quad (10)$$

Furthermore, though it is not necessary in the frequency shift calculation, one can keep

the one-body contribution of solvent region atoms to zero:

$$S_i = \begin{cases} \mathcal{N}(D(\tilde{\mathcal{R}})), & i \in \text{Probe} \\ \mathcal{N}(D(\tilde{\mathcal{R}})) - S_i^{(0)}, & i \in \text{Solvent} \end{cases} \quad (11)$$

$S_i^{(0)}$ is the one-body contribution to the frequency shift

$$S_i^{(0)} = \mathcal{N}(D(0)) \quad (12)$$

With the switch function of eqn. 10, the model excludes the interactions which not wanted based on different regions and distances between atoms. We tested four kinds of models named as different styles. The schematic is placed in Figure 1: *ae* is for a single atom, in here is the carbon atom of formic acid, selected as probe region with one-body contribution of water atoms modified as in eqn. 11, the name is from the keyword in the DeepMD-kit program.³² *atom* and *mol* styles are for a single atom and a single molecule atoms (here is formic acid) as probe region respectively. *regu* style is regular DP model with the switch function in eq. 9.

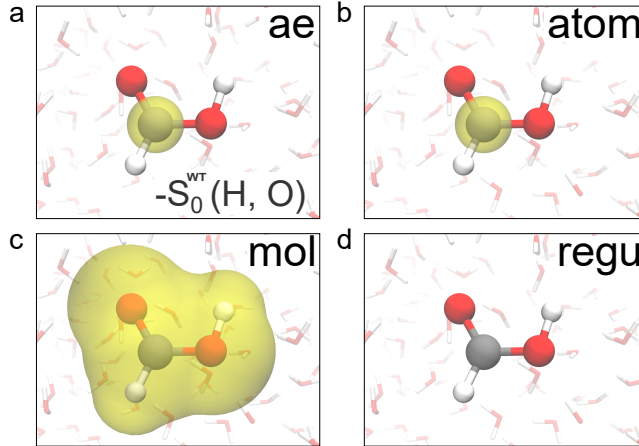


Figure 1: Schematic of four model styles. The molecule in center is formic acid surrounded by water molecules. Atoms in yellow bubble of *ae*, *atom*, and *mol* are selected as “probe region”. The minus term in *ae* means the isolated atomic contribution of water is subtracted (eq. 11). *regu* is the regular DP model.

However, one should note that these unwanted interactions still exist in the neural network as “atom types”, so if only one atom is taken as the probe region like in *atom* style, and only distances between the atom and other atoms will be counted. The final network expression still corresponds to a many-body form rather than a two-body form.

2.3 Computational details

For training and testing, all C=O stretching vibrational frequency shifts data of formic acid-water solution was calculated by the same protocol as in our previous work.¹⁴ Total 49999 frames in the trajectory were selected and calculated, 10 of them were dropped for self-consistent charge iterations convergence failure in energy calculation with GFN2.³³ Earlier 80% in MD trajectory, 39992 shifts were chosen as training data, and the left 20%, 9997 shifts were chosen as validation data and test data. After all frequency shifts were calculated, all data were given to a homemade code, which converted the data a format that can be read by DeePMD-kit program.

ae, *atom*, *mol* and *regu* styles were given two range settings. *s* and *l* (short and long) corresponds to 6 Å and 10 Å cut-range (R_{off}) respectively, R_{on} was set as 75% of R_{off} . Considering that atoms of same element may have different contributions, all atoms in the formic acid molecule entered into the program as different types. Other settings can be checked in the Supporting Information. All training progresses ran with DeepMD-kit v2.0.3 CPU version and 8 CPUs for parallel computing. Running time test results were obtained on the same data point and averaged over 1000 times.

3 Results and discussion

Four styles, two cut-range settings, in total eight models were tested in the prediction of frequency shifts. RMSEs results are summarized in Figure 2.

In all models, *mol/l* and *regu/l* gave the best results on RMSEs with about 6.5 cm⁻¹.

The worst result is on *ae/l* models, which gave RMSEs above 22 cm^{-1} , roughly equal to predict all shifts with the average value of the data, while *ae/s* gave a better result with 12.16 cm^{-1} .

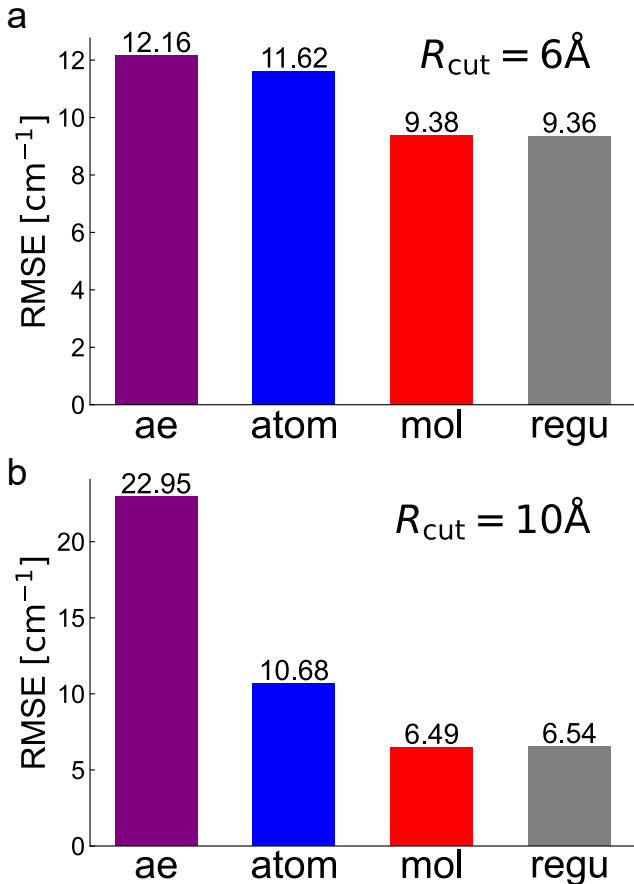


Figure 2: Root-mean-square errors in predicting frequency shifts with models of *ae*, *atom*, *mol*, *regu* styles, and different cut-ranges. R_{cut} is the interaction cut-off radius that corresponds to the R_{off} in eq. 10 and eq. 9.

RMSEs results of *ae* worse than *atom* show that atomic energy correction is unsuitable for shifts prediction. This can also explain why *ae* performed better with short cut-range, because the model with short cut-range has less atomic energy correction in model building. *atom* results are slightly worse than *mol*, which is easy to understand because *atom* has less probe region atoms than *mol*, which leads to a simpler network. And if the same cut-range is given, the extra probe region atoms in *mol* style will allow further solvent molecules to enter the net, so the networks of *mol* will contain more interactions. A possible additional

reason is that, as shown by Zhang et al.,³⁴ the network lacks completeness, and only one probe region atom makes the situation worse. *mol* style gave similar good results as *regu* style did in RMSEs, with about 6.5 cm^{-1} they can be used in accurate spectra simulation. There are two reasons why the *mol* style models can be smaller and good. First, in *regu* style, which is created for energy prediction, all interactions will be counted in the model. However, in the prediction of frequency shifts, only those interactions involved with the chromophore are essential. This is the idea within the design of *mol* style model, it does not contain solvent-solvent interactions explicitly. Second, the frequency shifts come from intramolecular motions that do not correspond to the vibrational mode and come from environmental effects,¹⁴ these environment effects have their limit range. If only considering non-bonded interactions between neutral molecules, the limit range is usually considered about 10 \AA . For a model that iterates through all atoms in system, like regular DP, a very large number of invalid atoms will be introduced into the network.

The comparison of error distribution is shown in Figure 3, distribution of errors with short cut-range is in Figure S1. The Kernel Density Estimate (KDE) plot of error distribution is in Figure 4. The RMSEs results and the error distributions are better with long cut-range. This trend is the same as in the training curves in Figure 6. As mentioned, the environment effects act on the chromophore have a limit range. We speculate that the accuracy will keep increasing as the distance increases until the limit is exceeded. Unfortunately, due to computer memory and time limitations, we cannot use a cut-range of more than 10 \AA . Our findings suggest that a distance larger than 6 \AA may increase accuracy.

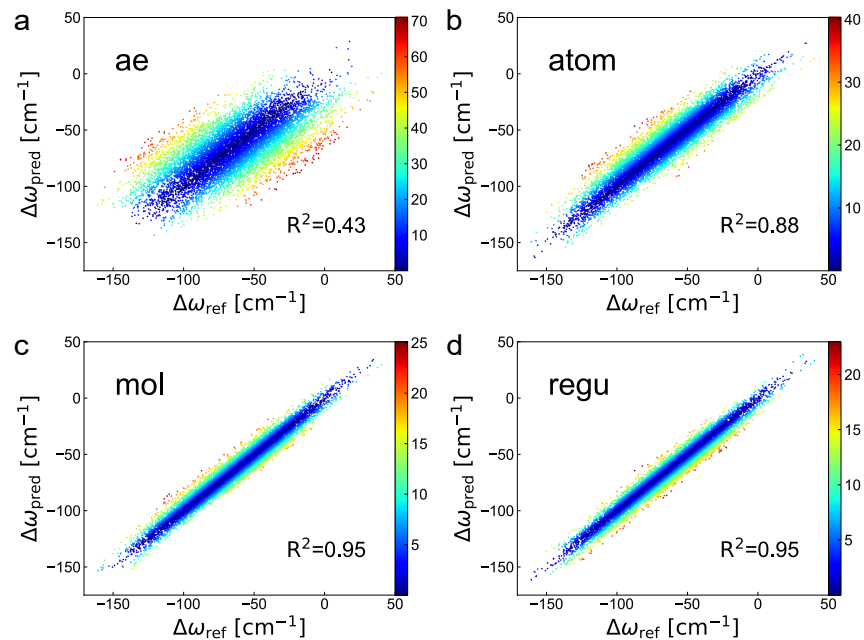


Figure 3: Error distribution in predicting frequency shifts with models of *ae*, *atom*, *mol*, *regu* styles and long cut-range of 10 Å. The color of points corresponds to the absolute error values.

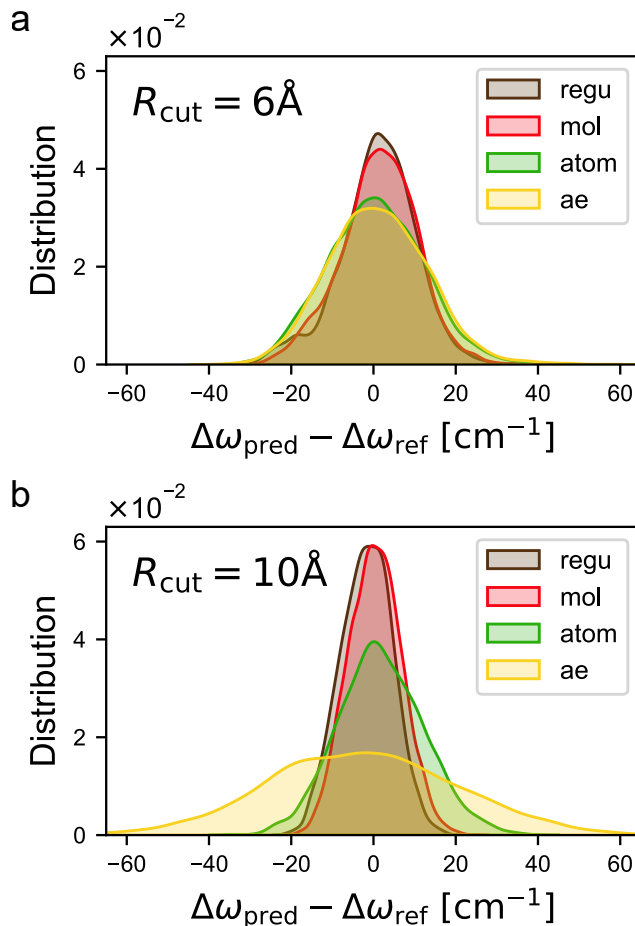


Figure 4: Kernel density estimate (KDE) plots of error distribution in predicting frequency shifts with models of *ae*, *atom*, *mol*, *regu* styles and different cut-ranges. R_{cut} is the interaction cut-off radius that corresponds to the R_{off} in eq. 10 and eq. 9.

On running time results shown in Fig. 5, there is no significant difference between *ae*, *atom*, and *mol* styles. *regu* style with biggest network gave above 2 seconds per data point, the slowest running time. In practice, taking the QVP method for example, requires five energy calculation tasks for each sampled trajectory frame, and with the GFN2 method, the total running time used on one particular frame can exceed 5 minutes. Running time results show that all models, including the slowest *regu* style models, are much faster than usual process.

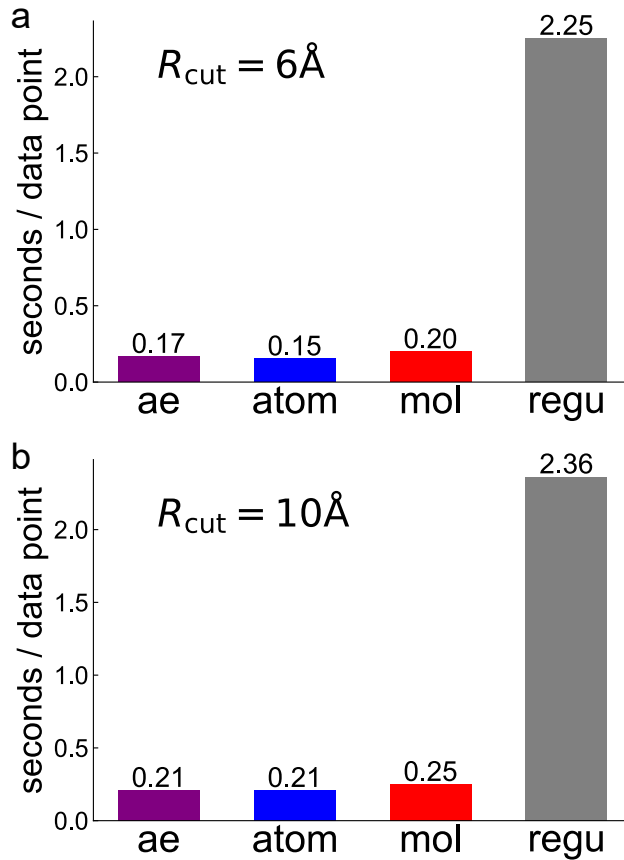


Figure 5: Running time of seconds per data point in predicting frequency shifts with models of *ae*, *atom*, *mol*, *regu* styles and different cut-ranges. R_{cut} is the interaction cut-off radius that corresponds to the R_{off} in eq. 10 and eq. 9.

However, these machine learning models can take a long time to train. The training time comparison is shown in Fig. 6. *regu* style takes more than two weeks to get a stable training result, which greatly limits its practical value for frequency calculation. In contrast, for *mol* style models, a stable result can be obtained within 100 hours, which shows that *mol* style model also meets the practical requirements in terms of training time.

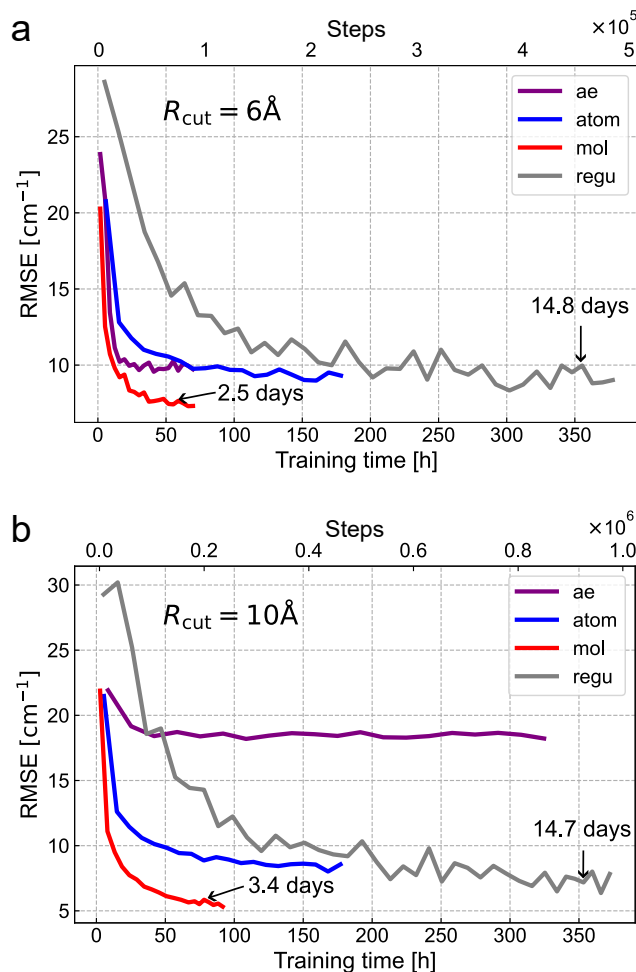


Figure 6: Training curve in predicting frequency shifts with models of *ae*, *atom*, *mol*, *regu* styles and different cut-ranges. R_{cut} is the interaction cut-off radius that corresponds to the R_{off} in eq. 10 and eq. 9. Results were smoothed for clarity.

4 Conclusion

In order to improve the computational efficiency of the vibrational spectrum simulation, we present a new machine learning method based on DPRc model. Rendered DPRc and DP model were utilized to calculate C=O stretching vibrational frequency shifts rather than potential. In order to reduce unnecessary information in solvent-solvent atomic interactions, we divided the system into a “probe region” and a “solvent region”. The inter-atomic distances in the “solvent region” are not counted in the neural network. Single atom with atomic

contribution correction, single atom and single molecule “probe region” were tested, we found that the accuracy of the single molecule “probe region” model is not reduced compared to the regular DP model, the running time is reduced to one-tenth or less of the regular DP model. The single molecule “probe region” model reduces the training time from more than two weeks to 3.4 days, which makes it fully applicable in practice.

Our results show that when using machine learning method to compute frequency shifts, dropping information on interactions between solvents can significantly increase computational and training efficiency while ensuring little loss of accuracy, which validates the design of focusing on chromophore. And interaction cut-off radii longer than 6 Å may need for higher accuracy.

The accuracy, training time, and running time of the single molecule “probe region” model meets the needs of practical spectral simulation. Our model can assist future long-time spectral sampling and vibrational modes coupling research. The model can be easily extended to calculate other physical quantities, such as dipole moments and polarizabilities, and simulate various spectra, such as Raman and sum frequency generation spectra.

Acknowledgement

This research was sponsored by the 2020-JCJQ Project (GFJQ2126-007) and the National Natural Science Foundation of China (Grants 22073035, 21773081, and 21533003).

Supporting Information Available

Error distribution of models at short cut-range and input files of 8 models which contain all parameters.

- SI.pdf: Error distribution at short cut-range.
- inputs.zip: Input files of 8 models

References

- (1) Cho, M. Coherent Two-Dimensional Optical Spectroscopy. *Chemical Reviews* **2008**, *108*, 1331–1418.
- (2) Nagata, Y.; Mukamel, S. Vibrational Sum-Frequency Generation Spectroscopy at the Water/Lipid Interface: Molecular Dynamics Simulation Study. *Journal of the American Chemical Society* **2010**, *132*, 6434–6442.
- (3) Schweitzer-Stenner, R. Advances in vibrational spectroscopy as a sensitive probe of peptide and protein structure: A critical review. *Vibrational Spectroscopy* **2006**, *42*, 98–117.
- (4) Rosenfeld, D. E.; Gengeliczki, Z.; Smith, B. J.; Stack, T. D. P.; Fayer, M. Structural dynamics of a catalytic monolayer probed by ultrafast 2D IR vibrational echoes. *Science (New York, N.Y.)* **2011**, *334*, 634–639.
- (5) Schauss, J.; Kundu, A.; Fingerhut, B. P.; Elsaesser, T. Contact Ion Pairs of Phosphate Groups in Water: Two-Dimensional Infrared Spectroscopy of Dimethyl Phosphate and ab Initio Simulations. *The Journal of Physical Chemistry Letters* **2019**, *10*, 6281–6286.
- (6) Roy, S.; Skoff, D.; Perroni, D. V.; Mondal, J.; Yethiraj, A.; Mahanthappa, M. K.; Zanni, M. T.; Skinner, J. L. Water Dynamics in Gyroid Phases of Self-Assembled Gemini Surfactants. *Journal of the American Chemical Society* **2016**, *138*, 2472–2475.
- (7) Salamatova, E.; Cunha, A.; Bloem, R.; Roeters, S.; Woutersen, S.; Jansen, T.; Pshenichnikov, M. Hydrophobic Collapse in N-Methylacetamide Water Mixtures. *The Journal of Physical Chemistry. A* **2018**, *122*, 2468–2478.
- (8) Ghosh, A.; Ostrander, J. S.; Zanni, M. T. Watching Proteins Wiggle: Mapping Structures with Two-Dimensional Infrared Spectroscopy. *Chemical Reviews* **2017**, *117*, 10726–10759.

- (9) Lin, Y.-S.; Shorb, J. M.; Mukherjee, P.; Zanni, M. T.; Skinner, J. L. Empirical Amide I Vibrational Frequency Map: Application to 2D-IR Line Shapes for Isotope-Edited Membrane Peptide Bundles. *The Journal of Physical Chemistry B* **2009**, *113*, 592–602.
- (10) Ham, S.; Kim, J.-H.; Lee, H.; Cho, M. Correlation between electronic and molecular structure distortions and vibrational properties. II. Amide I modes of NMA—nD₂O complexes. *The Journal of Chemical Physics* **2003**, *118*, 3491–3498.
- (11) la Cour Jansen, T.; Dijkstra, A. G.; Watson, T. M.; Hirst, J. D.; Knoester, J. Modeling the amide I bands of small peptides. *The Journal of Chemical Physics* **2006**, *125*, 044312.
- (12) Hayashi, T.; Zhuang, W.; Mukamel, S. Electrostatic DFT Map for the Complete Vibrational Amide Band of NMA. *The Journal of Physical Chemistry A* **2005**, *109*, 9747–9759.
- (13) Abramavicius, D.; Palmieri, B.; Voronine, D. V.; Šanda, F.; Mukamel, S. Coherent Multidimensional Optical Spectroscopy of Excitons in Molecular Aggregates; Quasiparticle versus Supermolecule Perspectives. *Chemical Reviews* **2009**, *109*, 2350–2408.
- (14) Cong, Y.; Zhai, Y.; Yang, J.; Grofe, A.; Gao, J.; Li, H. Quantum vibration perturbation approach with polyatomic probe in simulating infrared spectra. *Physical Chemistry Chemical Physics* **2022**, *24*, 1174–1182.
- (15) Zhao, R.; Shirley, J. C.; Lee, E.; Grofe, A.; Li, H.; Baiz, C. R.; Gao, J. Origin of thiocyanate spectral shifts in water and organic solvents. *The Journal of Chemical Physics* **2022**, *156*, 104106.
- (16) Yin, H.; Li, H.; Grofe, A.; Gao, J. Active-Site Heterogeneity of Lactate Dehydrogenase. *ACS Catalysis* **2019**, *9*, 4236–4246.

- (17) Olson, C. M.; Grofe, A.; Huber, C. J.; Spector, I. C.; Gao, J.; Massari, A. M. Enhanced vibrational solvatochromism and spectral diffusion by electron rich substituents on small molecule silanes. *The Journal of Chemical Physics* **2017**, *147*, 124302.
- (18) Xue, R.-J.; Grofe, A.; Yin, H.; Qu, Z.; Gao, J.; Li, H. Perturbation Approach for Computing Infrared Spectra of the Local Mode of Probe Molecules. *Journal of Chemical Theory and Computation* **2017**, *13*, 191–201.
- (19) Echave, J.; Clary, D. C. Potential optimized discrete variable representation. *Chemical Physics Letters* **1992**, *190*, 225–230.
- (20) Kwac, K.; Cho, M. Machine learning approach for describing vibrational solvatochromism. *Journal of Chemical Physics* **2020**, *152*.
- (21) Ye, S.; Zhang, G.; Jiang, J. AI-based spectroscopic monitoring of real-time interactions between SARS-CoV-2 and human ACE2. *Proceedings of the National Academy of Sciences of the United States of America* **2021**, *118*, 1–5.
- (22) Zhang, Y.; Ye, S.; Zhang, J.; Hu, C.; Jiang, J.; Jiang, B. Efficient and Accurate Simulations of Vibrational and Electronic Spectra with Symmetry-Preserving Neural Network Models for Tensorial Properties. *The Journal of Physical Chemistry B* **2020**, *124*, 7284–7290.
- (23) Ye, S.; Zhong, K.; Zhang, J.; Hu, W.; Hirst, J. D.; Zhang, G.; Mukamel, S.; Jiang, J. A machine learning protocol for predicting protein infrared spectra. *Journal of the American Chemical Society* **2020**, *142*, 19071–19077.
- (24) Gastegger, M.; Schütt, K. T.; Müller, K. R. Machine learning of solvent effects on molecular spectra and reactions. *Chemical Science* **2021**, *12*, 11473–11483.
- (25) Kananenka, A. A.; Yao, K.; Corcelli, S. A.; Skinner, J. L. Machine Learning for Vibra-

- tional Spectroscopic Maps. *Journal of Chemical Theory and Computation* **2019**, *15*, 6850–6858.
- (26) Kwac, K.; Freedman, H.; Cho, M. Machine Learning Approach for Describing Water OH Stretch Vibrations. *Journal of Chemical Theory and Computation* **2021**, *17*, 6353–6365.
- (27) Gao, J. Hybrid Quantum and Molecular Mechanical Simulations: An Alternative Avenue to Solvent Effects in Organic Chemistry. *Accounts of Chemical Research* **1996**, *29*, 298–305.
- (28) Ito, S.; Cui, Q. Multi-level free energy simulation with a staged transformation approach. *The Journal of Chemical Physics* **2020**, *153*, 044115.
- (29) Skinner, J. L.; Pieniazek, P. A.; Gruenbaum, S. M. Vibrational Spectroscopy of Water at Interfaces. *Accounts of Chemical Research* **2012**, *45*, 93–100.
- (30) Harris, D. O.; Engerholm, G. G.; Gwinn, W. D. Calculation of Matrix Elements for One-Dimensional Quantum-Mechanical Problems and the Application to Anharmonic Oscillators. *The Journal of Chemical Physics* **1965**, *43*, 1515–1517.
- (31) Zeng, J.; Giese, T. J.; Ekesan, ö.; York, D. M. Development of Range-Corrected Deep Learning Potentials for Fast, Accurate Quantum Mechanical/Molecular Mechanical Simulations of Chemical Reactions in Solution. *Journal of Chemical Theory and Computation* **2021**, *17*, 6993–7009.
- (32) Zhang, L.; Han, J.; Wang, H.; Saidi, W. A.; Car, R.; Weinan, E. End-to-end symmetry preserving inter-atomic potential energy model for finite and extended systems. *Advances in Neural Information Processing Systems* **2018**, *2018-Decem*, 4436–4446.
- (33) Bannwarth, C.; Ehlert, S.; Grimme, S. GFN2-xTB—An Accurate and Broadly Parametrized Self-Consistent Tight-Binding Quantum Chemical Method with Multi-

- pole Electrostatics and Density-Dependent Dispersion Contributions. *Journal of Chemical Theory and Computation* **2019**, *15*, 1652–1671.
- (34) Zhang, Y.; Xia, J.; Jiang, B. Physically-motivated Recursively Embedded Atom Neural Networks: Incorporating Local Completeness and Nonlocality. *Physical Review Letters* **2021**, *127*, 156002.

Graphical TOC Entry

